Journal of Microscopy, Vol. 229, Pt 3 2008, pp. 483–489
Received 26 September 2006; accepted 16 June 2007

Numerical study of optical nanolithography using nanoscale bow-tie–shaped nano-apertures

L. WANG & X. XU
School of Mechanical Engineering, Purdue University, West Lafayette, IN, U.S.A.

Key words. Bow-tie nano-aperture, FDTD, imaging contrast, nanolithography.

Summary

Contact lithography using bow-tie–shaped nano-apertures was recently demonstrated to achieve nanometer scale resolution. In this work, the detailed field distributions in contact nanolithography are analyzed using finite difference time domain simulations. It was found that the high imaging contrast, which is necessary for successful lithography, is achieved close to the mask exit plane and decays quickly with the increase of the distance from the mask exit plane. Simulations are also performed for comparable regular-shaped apertures and different shape bow-tie apertures. Design rules are proposed to optimize the bow-tie aperture for producing a sub-wavelength, high transmission field with high imaging contrast.

Introduction

Low-cost nanolithography techniques, such as near-field photolithography (Aizenberg *et al.*, 1997; Alkaisi *et al.*, 1999), nano-imprint lithography (Chou *et al.*, 1995), scanning probe lithography (Davy & Spajer, 1996) and surface plasmon–assisted nanolithography (Luo & Ishihara, 2004; Srituravanich *et al.*, 2004; Liu *et al.*, 2005), are generating a lot of interests recently. Standard photolithography techniques employ a light source to define patterns in the resist, and the minimum size of the features that can be obtained is limited to roughly half of the wavelength of the light (Madou, 1997). Advances in near-field optics using nanoscale light source have achieved spatial resolution significantly better than the diffraction limit (Rudman *et al.*, 1992; Inouye & Kawata, 1994). However, the transmission efficiency of commonly used regular shaped apertures, such as square or circular shaped apertures is very low (Bethe, 1944). Recently, numerical (Shi & Hesselink, 2002; Jin & Xu, 2004, 2005; Sendur *et al.*, 2004; Schuck *et al.*, 2005) and experimental studies (Chen *et al.*, 2003; Matteo *et al.*, 2004; Farahani *et al.*, 2005; Jin & Xu, 2006; Sundaramurthy *et al.*, 2006; Wang *et al.*, 2006; Xu *et al.*, 2006) have demonstrated high transmission and field concentration of certain types of ridge apertures, such as C, H and bow-tie–shaped apertures. These calculations showed that sub-wavelength apertures have the capability of confining light at visible wavelengths to sub-wavelength dimensions, along with transmission efficiency much higher than that of ordinary square- or circular-shaped apertures. Thus, these apertures offer great potentials in applications such as high-resolution imaging and optical data storage. Using these apertures as an alternative to the standard IC fabrication techniques for nanolithography is also attractive.

Recently, we have successfully demonstrated that nanoscale bow-tie apertures can be used for contact nanolithography to achieve nanometer scale resolution (Wang *et al.*, 2006). Bow-tie aperture has a longer cut-off wavelength than regular aperture does. Visible or UV light with proper polarization can pass through the bow-tie aperture without experiencing much intensity decay. The transmitted light is mainly confined underneath the tips of the bow tie, offering the optical resolution far beyond the diffraction limit.

Understanding the characteristics of near-field optical phenomena is an important step to improve the performance of nanolithography (McNab & Blaikie, 2000). In this paper, finite difference time domain (FDTD) simulations of light transmission through bow-tie nanoapertures are conducted to study the details of the transmitted near-field intensity and imaging contrast for lithography. Particularly, we focus our attention on the imaging contrast which is needed for successful lithography but has not received sufficient attention in the past studies. Our results show that, for nanolithography applications, the bow-tie–shaped nanoaperture has much better performance over conventional rectangular and square apertures with the same opening area. We also show that the imaging contrast and the transmitted near-field intensity strongly depend on the aperture dimension, tip separation, distance from the exit plane and the desired resolution to be obtained.

Correspondence to: X. Xu. Tel: 1 (765) 494 5639; fax: 1 (765) 494 6539; e-mail: xxu@ecn.purdue.edu

© 2008 The Authors
Journal compilation © 2008 The Royal Microscopical Society

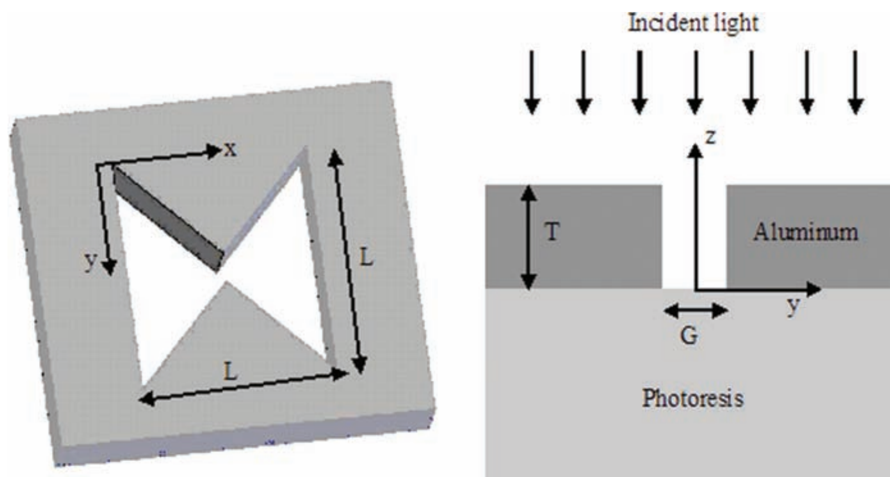

Fig. 1. Schematics of bow-tie aperture (left) and FDTD simulated structures (right). The grey area represents metal film.

Finite difference time domain simulations

It is well known that Fourier optics is no longer adequate for analyzing optical properties in real metals due to the finite skin depth, film thickness and surface plasmon effect (Goodman, 1996). Rigorous vectorial analysis must be applied. The FDTD numerical method simulates the optical near filed of light transmission through sub-wavelength apertures by numerically solving the Maxwell's equations. In this work, the FDTD method is used to compute the near-field distributions of a bow-tie aperture. The simulated geometry is shown in Fig. 1, which consists of a 150-nm-thick aluminium film mask and a semi-infinite photoresist layer. The bow-tie aperture has an L × L outline dimension with a tip separation distance of G. The wavelength of incident light is 355 nm and the electric field is polarized along the y direction. It is important to choose the right metal as the material of the opaque film, as it should have high reflection (to suppress the background light transmission through the metal film) and small skin depth (less loss for the light propagating through the aperture). Aluminium is selected as the film material because of its high reflectivity and small skin depth (reflectivity $R = 0.92$, skin depth = 6.5 nm) at the exposure wavelength of 355 nm. It is also shown to be stable in the ambient air environment during lithography process (Wang *et al.*, 2006).

The FDTD method was first introduced by Yee in 1966 (Yee, 1966). In FDTD algorithm, the computational region is discretized into small cubes, called Yee cells. Each cell has a dimension of Δx, Δy and Δz in Cartesian coordinates with size less than tenth of wavelength to ensure accurate numerical results. However, in the study of the near field of nanostructures, the cell size should be much smaller than the smallest dimensions of nanostructures to ensure the physical convergence, especially when the field quantities in the vicinity of the nanostructure is of interest. In this work, $4 \times 4 \times 4\ \text{nm}^3$ cells are used to model bow-tie nano-apertures. The stability condition relating the spatial and temporal step size is used, which is expressed as

$$v_{\max}\Delta t = \left[\frac{1}{\Delta x^2} + \frac{1}{\Delta y^2} + \frac{1}{\Delta z^2}\right]^{-1/2}, \tag{1}$$

where $v_{\max}$ is the maximum velocity of the wave in the material. In addition, absorbing or perfectly matched boundary conditions (Mur, 1981; Liao *et al.*, 2000) must be employed to eliminate the reflected waves on the boundaries of the finite computational domain and to ensure accurate results. The second-order absorbing boundary condition (Liao *et al.*, 2000) is used in this work. The commercial software package XFDTD 5.3 from Remcom is used, which has been used in many near-field calculations (Shi & Hesselink, 2002; Jin & Xu, 2004, 2005; Sendur *et al.*, 2004).

The modified Debye model is used to compute the complex permittivity for aluminium, which is expressed as

$$\varepsilon(\omega) = \varepsilon_\alpha + \frac{\varepsilon_5 - \varepsilon_\alpha}{1 + j\omega\tau} + \frac{\sigma}{j\omega\varepsilon_0}, \tag{2}$$

where ε_5 represents the static permittivity, $\varepsilon_\propto$ is the permittivity at infinite frequency which should be no less than 1, σ is conductivity and τ is the relaxation time. Given the experimental refractive index data of aluminium in the wavelength range of interest (Lide, 1996), the Debye model parameters are found as $\varepsilon_\propto = 1$, $\varepsilon_5 = -507.825$, $\tau = 9.398 \times 10^{-16}$ s and $\sigma = 4.8 \times 10^6\ \text{s m}^{-1}$. The index of refractive used for the photoresist is 1.6.

Results

The transmitted field intensity and imaging contrast (also called modulation) are two important factors for lithography patterning. Photoresist is sensitive to the total field intensity, and sufficient imaging contrast is needed for exposing the area that needs to be exposed for making good quality patterns

© 2008 The Authors

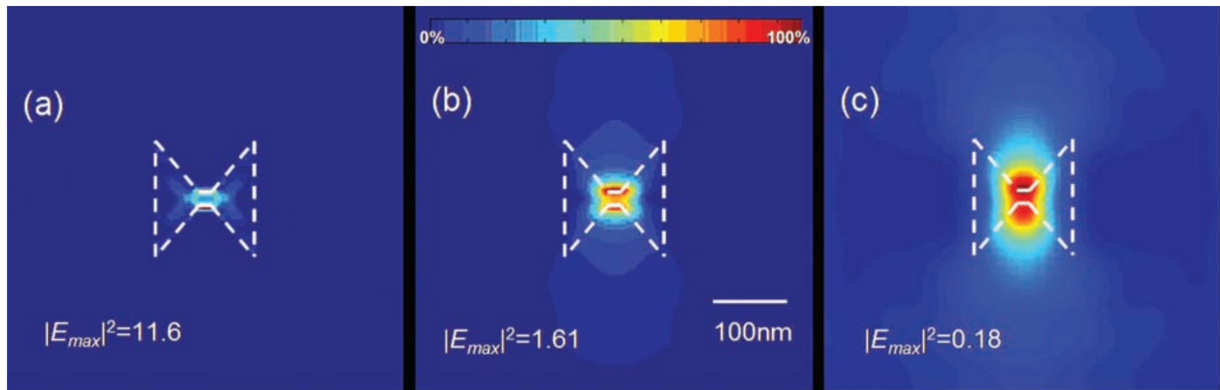

Fig. 2. Intensity distribution in the *x–y* plane of transmitted field of bow-tie aperture ($L = 160$ nm, $G = 24$ nm) at (a) 4 nm, (b) 16 nm and (c) 40 nm behind the exit plane

(Madou, 1997). In this report, these two factors are studied based on the simulation results. The imaging contrast $M(z, r)$ is defined as:

$$M(z, r) = \frac{I_{\max}(z) - I(z, r)}{I_{\max}(z) + I(z, r)}, \quad (3)$$

where z is the distance from the exit plane of the aperture and r is the radial coordinate. $I_{\max}(z)$ is the peak intensity of the light intensity in the plane with a distance z from the exit plane and $I(z,r)$ is the intensity where the imaging contrast needs to be evaluated.

Figures 2 and 3 show how the imaging contrast is calculated and used for estimating lithography performance, using the bow-tie antenna aperture as an example. The intensity distribution ($\sim E^2$) of the transmitted field in the *x–y* plane at distances (z) 4 nm, 16 nm and 40 nm behind the exit plane of the bow-tie aperture are shown. The intensity is normalized with the incident intensity, that is, the intensity of the incident wave is 1. The bow-tie aperture has the dimension of $L = 160$ nm and $G = 24$ nm. At a distance 4 nm from the exit plane, the maximum field intensity ($I_{\max}$) is found near the two tips of the bow-tie aperture. At a distance 12 nm from the exit plane, the field intensity has decreased considerably, and the highest intensity is at the centre ($r = 0$). This is true for any distance greater than 12 nm for this bow-tie aperture.

In this work, imaging contrasts are calculated at two radius, $r = 25$ nm and $r = 50$ nm at each distance, which is intended to find out if the imaging contrasts are sufficient for achieving lithography resolutions of 50 nm and 100 nm ($2r$). This is illustrated in Fig. 3, which shows the intensity profile across the centre of bow-tie aperture at 32 nm from the mask exit plane. $I_{\max}$ (=0.281) is located at the centre. The intensities at $r(x) =$ 25 nm and 50 nm are 0.180 and 0.049, respectively. From Eq. (3), the imaging contrasts at these two locations are calculated as 0.217 and 0.703. As shown in Fig. 3, the intensity difference between $I_{\max}$ and I ($r = 50$ nm) is much larger than that between $I_{\max}$ and I ($r = 25$ nm), which means it is much easier to control the total dose for fabricating a structure with a size of 100 nm than a size of 50 nm. The minimum imaging contrast required for exposing the S1805 photoresist, which has been used in nanolithography, is around 0.1 (Alkaisi *et al.*, 2000).

Once the field distribution and imaging contrast are calculated, we can also calculate a depth of focus (DOF) for achieving a specified resolution, which is the distance into the photoresist where light contrast is sufficient (>0.1) to expose the photoresist. In the following analysis, we calculate the DOF for achieving a 50 nm resolution.

Comparisons of bow tie, square and rectangular apertures

In this session, we discuss imaging contrasts and field intensities obtained from bow tie, square and rectangular apertures. A bow-tie aperture with 160 nm outline dimension (L) and 24 nm tip separation (G), a 115 nm × 115 nm square aperture (SQ) and a 320 nm × 40 nm rectangular aperture (REC) are computed. The dimensions of the square and the rectangular apertures are chosen to have the same opening area as the bow-tie aperture for the purpose of comparison. Table 1 summarizes the calculation results of spot size, transmission throughput, peak field intensities and DOF of 50 nm resolution. The spot size is defined as the full width at half magnitude (FWHM) of the intensity. The reason to show the results at 24 nm below the exit plane is that in lithography experiments, results are always observed with a certain depth. From the calculation results, it can be seen that the spot size of bow-tie aperture is smaller than those obtained from square and rectangular apertures. The transmission throughput is evaluated by the ratio of transmitted field intensity integrated over the aperture area to incident field intensity over the aperture area. The (normalized) peak field intensity is obtained at the centre of the aperture exit plane. It is found that the peak filed intensity of the bow-tie aperture is 2.82 times of rectangular aperture and 25 times of square aperture.

© 2008 The Authors
Journal compilation © 2008 The Royal Microscopical Society,

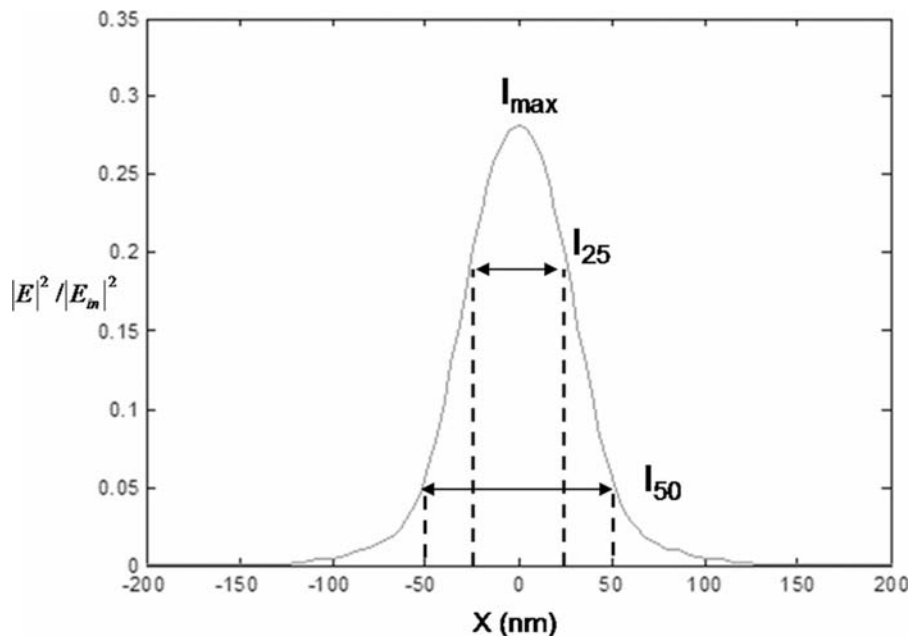

Fig. 3. Field intensity profile across the centre of the bow-tie aperture at 32 nm behind the exit plane.

The imaging contrasts for 50 nm resolution ($r = 25$ nm) in x–y plane as a function of depth z from the exit plane are shown in Fig. 4(a). It can be seen that the bow-tie aperture has the best contrast within 50 nm from the exit plane, and the contrast is less than that of a square aperture when the distance is larger than 50 nm. This is because the bow-tie aperture has the smallest spot size and the highest intensity when it is close to the mask exit plane, and its transmitted field diverges more quickly than rectangular and square apertures. Given the fact that the depth of nanolithography is normally less than 50 nm (Wang *et al.*, 2006), the bow-tie apertures offer the advantage for nanolithography in terms of having a higher imaging contrast.

Figure 4(b) shows the imaging contrast for 100 nm resolution. It is clear that all three apertures have much better contrast than those of 50 nm resolution. This means achieving 100 nm features is easier than achieving 50 nm features. Similar to 50 nm resolution, is also seen that the bow-tie aperture is better than square and rectangular apertures for 100 nm features patterning in terms of having a higher imaging contrast.

Comparisons of bow-tie apertures with different outline dimension

In this session, we discuss the size-dependent imaging contrasts and intensities of bow-tie nanoapertures. Four bow-tie apertures with different outline dimension (L): 120 nm, 160 nm, 200 nm and 300 nm are simulated. All other dimensions are chosen to be the same: a 24-nm tip separation and a 150-nm film thickness. Transmitted imaging contrasts for 50 nm and 100 nm resolution in the x–y plane as a function of depth z from the mask exit plane are studied.

Figures 5(a) and (b) show the imaging contrast for 50 nm and 100 nm resolution as a function of distance from the exit plane. We found that the contrasts of all the bow-tie apertures follow the same trends as the distance from the exit plane is increased. However, the imaging contrasts for 50 nm resolution are smaller than those of 100 nm resolution. This again indicates it is more difficult to achieve 50 nm resolution than 100 nm resolution.

A different bow-tie outline dimension can produce different transmitted power. The normalized peak field intensity, transmission throughput, DOF of 50 nm resolution and the

Table 1. Comparison of bow-tie and regular apertures.

	Bow-tie aperture	Rectangle	Square
Spot size at 24 nm in the photoresist	60 nm × 60 nm	136 nm × 152 nm	88 nm × 168 nm
Transmission throughput	1.19	1.83	0.2
Peak intensity	4.00	1.42	0.16
DOF of 50 nm resolution	60 nm	N/A	100 nm

© 2008 The Authors
Journal compilation © 2008 The Royal Microscopical Society,

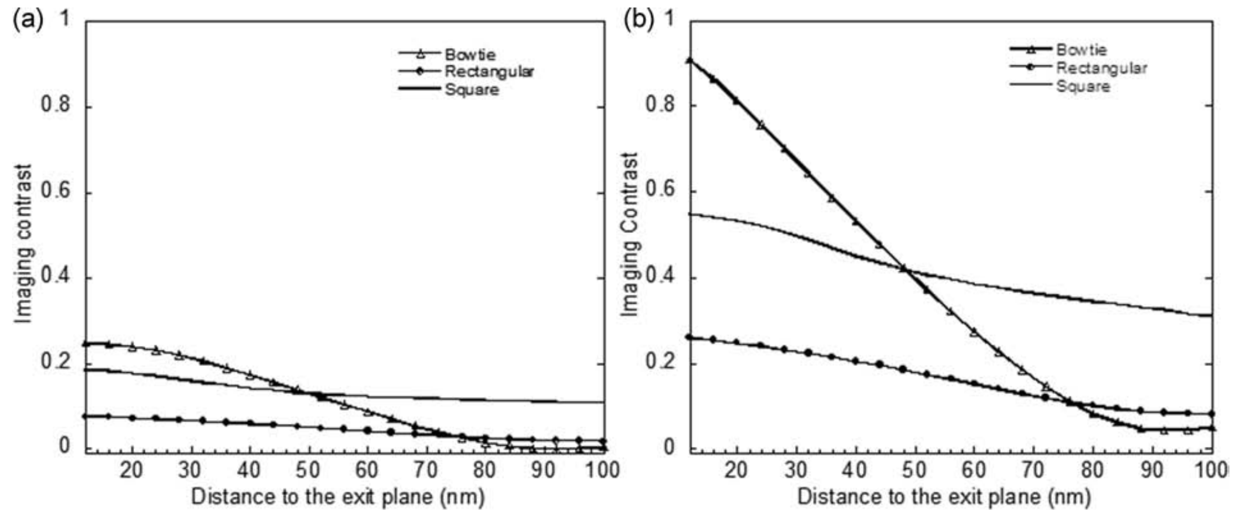

Fig. 4. Imaging contrast for (a) 50 nm and (b) 100 nm resolution in x–y plane as a function of depth z from the exit plane for bow tie, rectangular and square apertures.

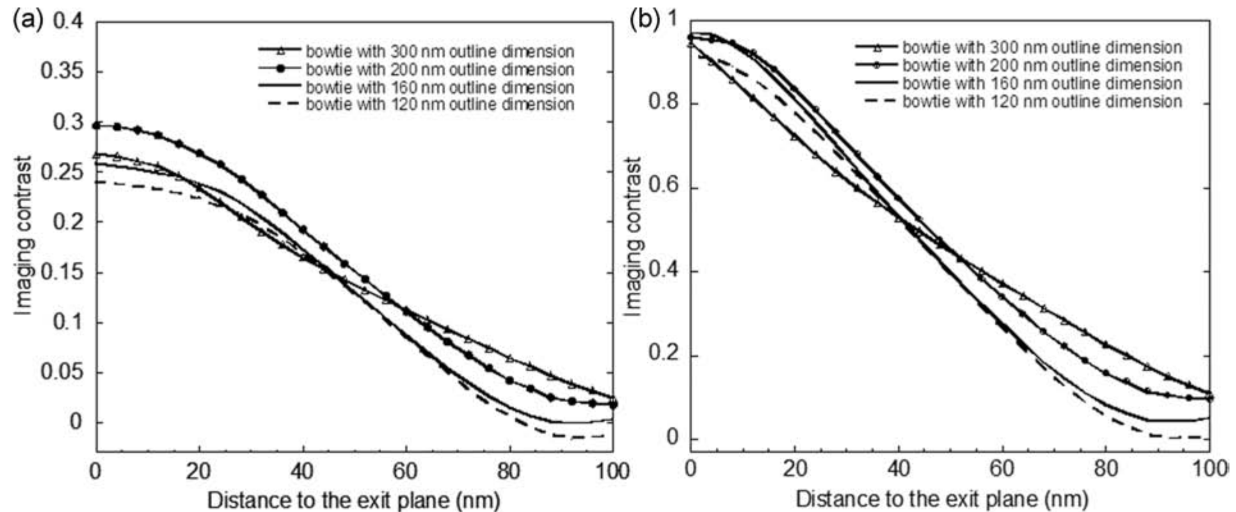

Fig. 5. Imaging contrast of (a) 50 nm and (b) 100 nm resolution as a function of depth z from the mask exit plane for bow-tie apertures having the same tip separation of 24 nm. Their outline dimensions are 300 nm, 200 nm, 160 nm and 120 nm.

spot size at 24 nm from the exit plane are summarized in Table 2. It is also found that a larger bow-tie aperture provides a higher field intensity. This is because as the aperture becomes larger, more light is able to be coupled into the aperture and to be focused by bow-tie aperture due to its light concentration function (Jin & Xu, 2005). The intensity is therefore enhanced. However, it is noticed that if the bow-tie aperture is larger than 160 nm, there is light leaking from the

Table 2. Comparison of different shape bow-tie apertures with same tip separation.

Bow-tie aperture outline dimensions	120 nm	160 nm	200 nm	300 nm
Spot size at 24 nm in the photoresist	60 nm × 80 nm	60 nm × 80 nm	60 nm × 88 nm	68 nm × 96 nm
Transmission throughput	1.77	1.19	0.89	0.62
Peak intensity	2.86	4.00	4.75	7.18
DOF of 50 nm resolution	56 nm	57 nm	61 nm	62 nm

two arms of the aperture and the transmitted spot size starts to be elongated in y direction. Thus, carefully selecting the aperture size is necessary to achieve both field enhancement and concentration. The calculation results show that the optimum size of the bow-tie outline dimension is around half of the incident wavelength.

Comparison of bow-tie apertures with different tip separations

We also calculated transmitted near-field intensities of bow-tie apertures with various tip separation distances. Three bow-tie apertures are simulated with tip separation distance of 32 nm, 24 nm and 16 nm. All of them have the same outline dimensions of 160 nm. In Fig. 6(a), the imaging contrast is calculated for 50 nm resolution. We found that these bow-tie apertures provide very limited intensity contrast, except the one with the smallest tip separation. Figure 6(b) shows the intensity contrast for 100 nm resolution. The imaging contrasts follow the same trend, and high imaging contrasts can be obtained for all three bow-tie apertures since the tip separation sizes are all much smaller than 100 nm. The bow-tie aperture with the smaller tip separation distance has slightly better contrast. Comparing Figs 6(a) and (b), it is seen again that achieving 50 nm resolution is much more difficult than achieving 100 nm resolution in terms of imaging contrast.

Table 3 summarized the normalized peak field intensity, transmission throughput, DOF of 50 nm resolution and the spot size at 24 nm from the exit plane. It can be seen that the spot size becomes smaller and the peak field intensity increases with the decreasing of tip separation. This is because the transmitted field is essentially induced by the dipole radiation, which has opposite charges at the two bow-tie tips. The reduction of tip separation increases the charge density due to the stronger coupling between the two tips, which increases the transmitted near-field intensity.

From the above discussions based on the calculations results, it can be concluded that to design nanoscale bow-tie apertures for producing a sub-wavelength, high transmission field with high imaging contrast, its outline dimension and tip separation are two important parameters. A large aperture area can increase the light throughput, however, its length should be less than half the wavelength in order to avoid light leaking from the arms. On the other hand, a small tip separation can concentrate the light spot and increase the imaging contrast. These two can be used as a general design rule for using bow-tie apertures for nanolithography. On the other hand, there are many process difficulties to overcome, such as accurate fabrication of bow-tie apertures and maintaining an intimate contact between the mask and the photoresist. These factors do set a practical limit, and need to be taken into account in actual lithography work.

Table 3. Comparison of different shape bow-tie apertures with same outline dimensions.

Tip separation	32 nm	24 nm	16 nm
Spot size at 24 nm in the photoresist	72 nm × 96 nm	60 nm × 80 nm	48 nm × 56 nm
Transmission throughput	1.15	1.19	1.26
Peak intensity	2.01	4.00	10.24
DOF of 50 nm resolution	57 nm	57 nm	57 nm

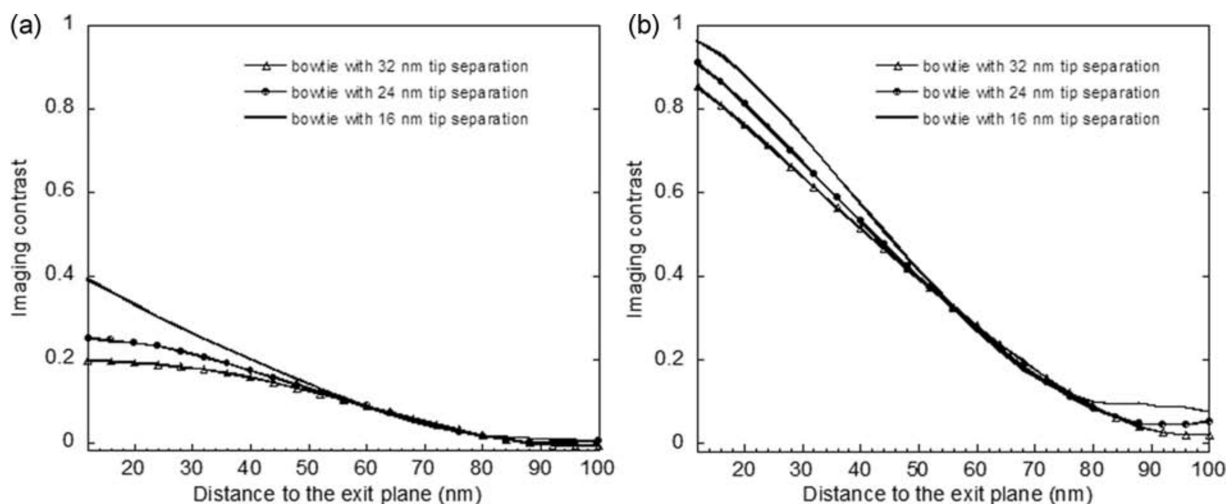

Fig. 6. (a) 50 nm and (b) 100 nm resolution imaging contrast for bow-tie apertures with tip separation sizes of 32 nm, 24 nm and 16 nm.

© 2008 The Authors
Journal compilation © 2008 The Royal Microscopical Society,

Conclusions

Imaging contrast and field intensity in nanolithography using bow-tie apertures were investigated by computer simulations. Results demonstrated that bow-tie apertures provide both higher transmitted field intensity and smaller spot size than comparable regularly shaped apertures. We also analyzed the imaging contrast and field intensity for achieving 50 and 100 nm resolutions by varying bow-tie aperture dimension and tip separation. It was found that achieving 50 nm lithography resolution is much more difficult than achieving 100 nm resolution because of much smaller imaging contrast values. Given the fact that the minimum imaging contrast required for exposing the S1805 photoresist is 0.1, the depth of focus for exposing 50 nm features by different shaped nanoscale apertures with different shapes are also calculated. The combination of a large outline dimension close to half the wavelength and a smallest tip separation allows the transmitted field intensity and imaging contrast of bow-tie aperture to be optimized.

Acknowledgement

This work was performed with the support of the National Science Foundation.

References

Aizenberg, J., Rogers, J.A., Paul, K.E. & Whitesides, G.M. (1997) Imaging the irradiance distribution in the optical near field. *Appl. Phys. Lett.* **71**, 3773–3775.

Alkaisi, M.M., Blaikie, R.J. & McNab, S.J. (2000) 70 nm features on 140 nm period using evanescent near field optical lithography. *Microelect. Eng.* **53**, 236–240.

Alkaisi, M.M., Blaikie, R.J., McNab, S.J., Cheung, R. & Cumming, D.R.S. (1999) Sub-diffraction-limited patterning using evanescent near-field optical lithography. *Appl. Phys. Lett.* **75**, 3560–3562.

Bethe, H. (1944) Theory of diffraction by small holes. *Phys. Rev.* **66**, 163–182.

Chen, F., Itagi, A., Bain, J., *et al.* (2003) Imaging of optical field confinement in ridge waveguides fabricated on very-small-aperture laser. *Appl. Phys. Lett.* **83**, 3245–3247.

Chou, S.Y., Krauss, P.R. & Renstrom, P.J. (1995) Imprint of sub-25 nm vias and trenches in polymers. *Appl. Phys. Lett.* **67**, 3114–3116.

Davy, S. & Spajer, M. (1996) Near field optics: snapshot of the field emitted by a nanosource using a photosensitive polymer. *Appl. Phys. Lett.* **69**, 3306–3308.

Farahani, J.N., Pohl, D.W., Eisler, H.J. & Hecht, B. (2005) Single quantum dot coupled to a scanning optical antenna: a tunable superemitter. *Phys. Rev. Lett.* **95**, 017402.

Goodman, J.W. (1996) *Introduction to Fourier Optics*, 2nd edn., Chap. 3, McGraw-Hill, New York.

Inouye, Y. & Kawata, S. (1994) Near-field scanning optical microscope with a metallic probe tip. *Opt. Lett.* **19**, 159–161.

Jin, E.X. & Xu, X. (2004) Finite-difference time-domain studies on optical transmission through planar nano-apertures in a metal Film. *Jpn. J. Appl. Phys.* **43**, 407–417.

Jin, E.X. & Xu, X. (2005) Obtaining super resolution light spot using surface plasmon assisted sharp ridge nanoaperture. *Appl. Phys. Lett.* **86**, 111106.

Jin, E.X. & Xu, X. (2006) Enhanced optical near field from a bowtie aperture. *Appl. Phys. Lett.* **88**, 153110.

Liao, Z.P., Wong, H.L., Yang, B. & Yuan, Y. (1984) A transmitting boundary for transient wave analysis. *Scientia Sinica* **28**, 1063–1076.

Lide, D.R. (1996) *CRC Handbook of Chemistry and Physics*, Vol. 12, 77th edn., CRC Press, Boca Raton, Florida.

Liu, Z., Wei, Q. & Zhang, X. (2005) Surface plasmon interference nanolithography. *Nano. Lett.* **5**, 957–961.

Luo, X. & Ishihara, T. (2004) Surface plasmon resonant interference nanolithography technique. *Appl. Phys. Lett.* **84**, 4780–4782.

McNab, S.J. & Blaikie, R.J. (2000) Contrast in the evanescent near field of $\lambda/20$ period gratings for photolithography. *Appl. Opt.* **39**, 21–25.

Madou, M.J. (1997) *Fundamentals of Microfabrication*. CRC Press, Boca Raton, Florida.

Matteo, J.A., Fromm, D.P., Yuen, Y., Schuck, P.J., Moerner, W.E. & Hesselink, L. (2004) Spectral analysis of strongly enhanced visible light transmission through single C-shaped nanoapertures. *Appl. Phys. Lett.* **85**, 648–650.

Mur, G. (1981) Absorbing boundary conditions for the finite-difference approximation of the time-domain electromagnetic-field equations. IEEE Trans Electromagn Compat **23**, 377–382.

Rudman, M., Lewis, A., Mallul, A., Haviv, V., Turovets, I., Shchemelinin, A. & Nebenzahl, I. (1992) Near-field photolithography with a solid immersion lens. *J. Appl. Phys.* **72**, 4379.

Schuck, P.J., Fromm, D.P., Sundaramurthy, A., Kino, G.S. & Moerner, W.E. (2005) Improving the mismatch between light and nanoscale objects with gold bowtie nanoantennas. *Phys. Rev. Lett.* **94**, 017402.

Sendur, K., Challener, W. & Peng, C. (2004) Ridge waveguide as a near-field aperture for high density data storage. *J. Appl. Phys.* **96**, 2743–2752.

Shi, X. & Hesselink, L. (2002) Mechanisms for enhancing power throughput from planar nano-apertures for near-field optical data storage. *Jpn. J. Appl. Phys.* **41**, 1632–1635.

Srituravanich, W., Fang, N., Sun, C., Luo, Q. & Zhang, X. (2004) Plasmonic nanolithography. *Nano. Lett.* **4**, 1085–1088.

Sundaramurthy, A., Schuck, P.J., Conley, N.R., Fromm, D.P., Kino, G.S. & Moerner, W.E. (2006) Toward nanometer-scale optical photolithography: utilizing the near-field of bowtie optical nanoantennas. *Nano. Lett.* **6**, 355–360.

Wang, L., Uppuluri, S.M., Jin, E.X. & Xu, X. (2006) Nanolithography using high transmission nanoscale bowtie apertures. *Nano. Lett.* **6**, 361–364.

Xu, X., Jin, E.X., Wang, L. & Uppuluri, S.M. (2006) Design, fabrication, and characterization of nanometer-scale ridged aperture optical antenna. *Proc. SPIE* **6106**, 61061J.

Yee, K. (1966) Numerical solutions of initial boundary value problems involving Maxwell's equations in isotropic media. *IEEE Trans Antennas Propagation* **14**, 302–307.

© 2008 The Authors
Journal compilation © 2008 The Royal Microscopical Society,